Biomaterials Advances 159 (2024) 213800

Contents lists available at ScienceDirect

Biomaterials Advances

journal homepage: www.journals.elsevier.com/materials-science-and-engineering-c

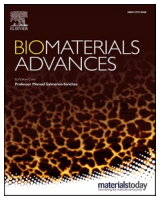

# Uncovering the relationship between macrophages and polypropylene surgical mesh

Nicholas T.H. Farr [a,b,*,1], Victoria L. Workman [a,b,1], Sanad Saad [a,c,1], Sabiniano Roman [a], Vanessa Hearnden [a,b], Christopher R. Chapple [d], Craig Murdoch [e], Cornelia Rodenburg [a,b], Sheila MacNeil [a]

[a] Department of Materials Science and Engineering, University of Sheffield, Sir Robert Hadfield Building, Mappin Street, Sheffield, UK
[b] Insigneo Institute for in silico Medicine, The Pam Liversidge Building, Sir Robert Hadfield Building, Mappin Street, Sheffield, UK
[c] Department of Urology, Sheffield Teaching Hospitals NHS Foundation Trust, Sheffield, UK
[d] Department of Urology, Royal Hallamshire Hospital, Urology Clinic, Sheffield, UK
[e] School of Clinical Dentistry, 19 Claremont Crescent, University of Sheffield, Sheffield, UK

ARTICLE INFO

*Keywords:*
In vitro biological models
Biomolecular Engineering
Tissue engineering
Biomaterials
Preclinical testing
Surface analysis

ABSTRACT

Currently, *in vitro* testing examines the cytotoxicity of biomaterials but fails to consider how materials respond to mechanical forces and the immune response to them; both are crucial for successful long-term implantation. A notable example of this failure is polypropylene mid-urethral mesh used in the treatment of stress urinary incontinence (SUI). The mesh was largely successful in abdominal hernia repair but produced significant complications when repurposed to treat SUI. Developing more physiologically relevant *in vitro* test models would allow more physiologically relevant data to be collected about how biomaterials will interact with the body. This study investigates the effects of mechanochemical distress (a combination of oxidation and mechanical distention) on polypropylene mesh surfaces and the effect this has on macrophage gene expression. Surface topology of the mesh was characterised using SEM and AFM; ATR-FTIR, EDX and Raman spectroscopy was applied to detect surface oxidation and structural molecular alterations. Uniaxial mechanical testing was performed to reveal any bulk mechanical changes. RT-qPCR of selected pro-fibrotic and pro-inflammatory genes was carried out on macrophages cultured on control and mechanochemically distressed PP mesh. Following exposure to mechanochemical distress the mesh surface was observed to crack and craze and helical defects were detected in the polymer backbone. Surface oxidation of the mesh was seen after macrophage attachment for 7 days. These changes in mesh surface triggered modified gene expression in macrophages. Pro-fibrotic and pro-inflammatory genes were upregulated after macrophages were cultured on mechanochemically distressed mesh, whereas the same genes were down-regulated in macrophages exposed to control mesh. This study highlights the relationship between macrophages and polypropylene surgical mesh, thus offering more insight into the fate of an implanted material than existing *in vitro* testing.

## 1. Introduction

Providing a realistic *in vitro* environment for biomaterials testing has been and continues to be challenging. Biomaterials performing well during *in vitro* testing, but failing to replicate their success in clinical trials are unfortunately common [1]. It has been established that the major reasons for biomaterial failure include wear/corrosion, fibrous encapsulation, inflammation, low fatigue strength and mismatch in modulus between native tissues and implants [2]. Despite studies identifying and evaluating such failure modes *in vitro* testing of biomaterial implants is still lagging behind [3]. Current ISO standards focus on *in vitro* assessment of cytotoxicity and immunogenicity is only evaluated using animal testing. Additionally, *in vitro* evaluation of biomaterials is carried out under static conditions whereas most biomaterial implants are deployed in an ever changing physiological environment, which can lead to failure due to wear and fatigue. Implanted biomaterials change

* Corresponding author at: Department of Materials Science and Engineering, University of Sheffield, Sir Robert Hadfield Building, Mappin Street, Sheffield, UK.
*E-mail address:* n.t.farr@sheffield.ac.uk (N.T.H. Farr).
[1] These authors contributed equally to this work.

https://doi.org/10.1016/j.bioadv.2024.213800
Received 29 August 2023; Received in revised form 6 February 2024; Accepted 11 February 2024
Available online 15 February 2024

over time in the body but this effect is difficult to replicate *in vitro*. Our previous work has shown that subjecting several biomaterials used in the pelvic floor to dynamic strain *in vitro* significantly changes their mechanical properties and surface chemistry after only 3 days [4]. It has been hypothesised that these changes adversely affect the clinical response to biomaterials and ultimately lead to failure of implants [5]. There are still no prescribed *in vitro* testing methods examining the effects of mechanical and oxidative stress on biomaterial implants.

An example of where materials selection has not been designed to consider the implantation environment is the use of polypropylene (PP) surgical mesh for pelvic floor repair. A review of the literature reveals that this biomaterial was introduced into clinical practice without either adequate preclinical testing in an animal model of the pelvic floor or long term clinical studies [6]. Despite having been used with a high degree of success in the abdomen for hernia repair PP use to support pelvic organs has led to severe complications. The success of PP surgical mesh appears to be highly dependent on its implantation site, both in terms of mechanical and oxidative environments. The assumption that a material performing well in one site in the body will perform equally well elsewhere has not stood the test of time [7]. The reasons for complications in the pelvic floor environment are not clearly understood, but may be twofold: (i) a mechanical mismatch between the mesh and the native tissues; and (ii) the fibres of the mesh provoking an adverse cellular response or indeed both [8]. An *in vitro* model is required that brings together mechanical distension and immunological interrogation.

A recent biomechanics analysis considered various forms of loading experienced by mesh in the pelvic floor to explain why the material fails. Current evidence proved inconclusive and the author concluded that more work needs to be done to quantify the mechanical behaviour of surgical mesh materials to better understand why these materials fail [9]. To that end recent studies from our laboratory used an *in vitro* bioreactor to subject PP surgical mesh to oxidative stress *via* hydrogen peroxide and mechanical stress by repetitive cyclic uniaxial distension [5]. This combination of mechanical and oxidative stresses has been termed "mechanochemical" distress, the application of which significantly affected the surface properties of PP surgical mesh [10].

All implanted materials initiate an immune response, leading to a short period of inflammation that becomes attenuated within a few weeks. However, in some cases the material, because of its inherent degradability or toxicity, leads to prolonged, chronic inflammation with the cells of the immune system seeking to reject the implanted foreign material [11]. Macrophages are resident immune cells within tissues or are differentiated from circulating monocytes that extravasate into tissues from the bloodstream [12]. They exhibit remarkable plasticity and exist on a diverse phenotypic spectrum [12]. Macrophages initially attempt to phagocytose implanted material, however if the implant is too large to engulf a phenomenon known as frustrated phagocytosis occurs whereby macrophages release degradative enzymes and reactive oxygen species to enable disintegration of the biomaterial into smaller fragments that can then be engulfed [13]. This hostile inflammatory environment can lead to surface changes in the biomaterial [14,15]. Recent studies have now provided greater insights into how macrophages interact with surgical mesh *in vivo* [16,17].

In order to create a model that incorporates mechanochemical distress with interrogation by macrophages we cultured macrophages on PP mesh that had previously been subjected to oxidative stress *via* hydrogen peroxide and mechanical stress by repetitive cyclic uniaxial distension. To evaluate the effect of macrophages on PP surgical mesh before and after mechanochemical distress we examined macrophage gene transcription responses by selecting a number of genes commonly found to be dysregulated in inflammation or biomaterial-induced fibrosis [18–28]. In addition, various surface characterisation techniques, such as SEM, AFM, EDX, ATR-FTIR and Raman spectroscopy were used to detect changes in the PP mesh and uniaxial tensile testing was performed to reveal bulk mechanical changes. This study links mechanochemical distress with an initial macrophage response through the use of sensitive surface analysis techniques and RT-qPCR of key genes.

## 2. Materials and methods

### 2.1. Sample preparation

Strips of commercially available PP surgical mesh, (Prolene® Mesh, Ethicon, Belgium), were cut into 1.5 cm × 1.5 cm strips using sterilised scissors within a cell culture cabinet along the longitudinal direction of the surgical mesh. PP mesh samples were clamped between the grips of an Ebers bioreactor (Ebers Medical Technology SL, Zaragoza, Spain). The length of sample subjected to mechanical forces was 1.2 cm, with approximately 11 pores present. Samples were immersed in 3 % *v*/v hydrogen peroxide solution (hydrogen peroxide solution, contains inhibitor, 30 wt% in $H_2O$, Sigma-Aldrich). Samples were subjected to 25 % repetitive cyclic uniaxial distension at a frequency of 0.5 cycles per minute at 37 °C. When taking into account the maximum abdominal pressure, the maximum theoretical strength per unit width of a hernia mesh should be 16 N/cm for a small hernia. Lightweight meshes have an elasticity in the range of 20–35 % at 16 N/cm [29], and it is suggested that lower elasticity would restrict abdominal distention (*i.e.* mean distension of the abdominal wall at 16 N/cm is around 25 % depending on the direction). The 25 % distension selected for this study thus represents high mechanical stress on the fibres. A high-end physiological distention (25 %), only experienced during sneezing for instance, was used with a high repetition pattern for the purposes of an accelerated/fatigue model. These samples are then referred to as mechanochemically distressed samples throughout this study. Cells were not cultured on the mesh at any point during mechanochemical distension.

### 2.2. Cell isolation and culture

Human monocytes were isolated from leukocyte-enriched buffy coats obtained from healthy blood donors (purchased from NHS Blood and Transplant). Blood was diluted 1:1 with HBSS without calcium and magnesium (Thermofisher Scientific, UK), layered on Ficoll-Paque Plus (Amersham Biosciences, UK) and centrifuged for 40 min at 400 x*g*. The mononuclear cell-rich layer was removed, washed twice with HBSS, and resuspended in IMDM (Lonza, UK) supplemented with 2 % human AB serum (Merck, UK), 100 IU/ml penicillin and 100 mg/ml streptomycin (Sigma-Aldrich, UK). Mononuclear cells were seeded at $8 \times 10^7$ cells into 10 $cm^2$ tissue culture plates and cultured overnight after which nonadherent cells were removed by washing three times with HBSS and the culture medium replenished. To generate fully differentiated monocyte-derived macrophages (MDM), adherent monocytes were cultured for 7 days [30]. Macrophages were then gently removed from tissue culture plates with a cell scraper (Thermofisher, UK) and seeded at a density of $1 \times 10^6$ cells per sample on tissue culture plastic, control or mechanochemically distressed mesh. Samples were cultured for a further 7 days before proceeding to RNA extraction. Macrophages cultured on tissue culture plastic designated M-TCP.

### 2.3. Experimental design

Samples were prepared as described in Table 1 and physical, chemical and immunogenetic testing carried out as described in Fig. 1.

### 2.4. Low voltage (LV)-scanning electron microscopy imaging

FEI Helios Nanolab G3 (FEI Company, US) and Helios G4 DualBeam (ThermoFisher Scientific, US) microscopes were employed for surface morphology observations of mesh samples. In contrast to common scanning electron microscopy (SEM) analysis practice, samples were not pre-treated with a conductive coating by deposition. An accelerating voltage of 1–2 keV at typical chamber vacuum pressures in the range of

**Table 1**
Description of samples and the conditions used in their preparation.

| Sample ID | PP surgical mesh | Cell culture | Analyses performed | |
|---|---|---|---|---|
| | | | Physical and Chemical Properties | Immuno-genetic |
| Control PP | As supplied | – | Yes | – |
| Mechanochemically distressed PP | Repetitive 25 % distension for 72 h then incubated in 3 % $H_2O_2$ at 37 °C | – | Yes | – |
| Tissue culture plastic + macrophages | – | 7 days | – | Yes |
| Control PP + macrophages | As supplied | 7 days | Yes | Yes |
| Mechanochemically distressed PP + macrophages | Repetitive 25 % distension for 72 h then incubated in 3 % $H_2O_2$ at 37 °C | 7 days | Yes | Yes |

$10^{-6}$ mbar and a working distance of 4 mm were chosen to avoid sample damage through surface charging. An Everhart-Thornley Detector (ETD) was selected for low magnification of SE images and a Through Lens Detector (TLD) for high magnification SE images.

### 2.5. Energy dispersive X-ray spectroscopy (EDX)

FEI Nova nanoSEM 450 (FEI Company, USA) SEM equipped with an Energy Dispersive X-ray Spectroscopy (EDX) detector (Oxford Instruments, UK) was used to capture EDX spectra. EDX spectra were taken from the centre of each PP fibre to mitigate any effects associated with fibre orientation. The spectra were obtained with a 10 keV accelerating voltage using a 4.5 spot probe current at a working distance of 5 mm. Data analysis was automated by the application of Aztec EDX analysis software (Oxford Instruments, UK).

### 2.6. Atomic force microscopy

Atomic force microscopy (AFM) microscopy was performed in tapping mode with SCANASYST-AIR probes under ambient conditions on a Bruker Dimension Icon AFM. PP mesh samples were placed on a cover glass and then attached to a magnetic AFM support. Different areas of the samples were analysed to produce peak force images obtained through PeakForce Tapping AFM mode, where the maximum value of the tip-surface interaction force is used as a constant setpoint for each pixel of the area scanned [31]. Data analysis was performed using Bruckers NanoScope Analysis software (Version 2.0).

### 2.7. Attenuated total reflectance - Fourier-transform infrared spectroscopy

Infrared spectra were obtained for all test mesh samples with a NICOLET 380 Fourier-transform infrared (FTIR) spectrometer (ThermoFisher Scientific, US). Samples were purged with dry air before spectra collection in the range from 500 to 4000 $cm^{-1}$ averaging 32 scans and a resolution of 4 $cm^{-1}$. The samples were washed in three consecutive lots of $dH_20$ to remove any residual cells and extracellular matrix (ECM), and then analysed in their solid state form using an attenuated total reflection (ATR) accessory with a Golden Gate® diamond crystal (Specac, UK).

### 2.8. Raman spectroscopy

Raman spectroscopy (Renishaw inVia micro-Raman) was employed to analyse the chemical structure of control and mechanochemically distressed PP mesh samples. Raman spectra were collected from longitudinal washed ($dH^20$) fibres located distal to mesh knot sites. A 50× objective was selected with 10 s exposure. The laser power was set at 3 Mw with a 1 μm spot size. A Peltier-cooled multichannel CCD detector was used for data recording with a 2400 lines/mm diffraction grating at a slit opening of 65 μm and a spectral resolution of in the order of 1 $cm^{-1}$. For data analysis no smoothing was applied with baseline subtraction performed using OriginLab (OriginLab Corporation, US) software.

### 2.9. Uniaxial tensile testing

Uniaxial ramp testing was performed for all mesh samples sets. A tensiometer (MultiTest-dV, Mecmesin) was used with test pieces ($n = 3$, for each material). Samples (1 cm × 1.5 cm strips) were clamped between two grips of the tensiometer with a testing length of 10 mm. A load cell of 250 N was used. The sample meshes test pieces were loaded in the longitudinal direction, in the direction of use as indicated by the manufacturer. A tensile test was then applied at a rate of 0.1 mm $s^{-1}$. All experiments were performed under constant laboratory conditions (23 °C, British air humidity 80 %).

### 2.10. Extraction and quantification of macrophage RNA

#### 2.10.1. RNA extraction

RNA was extracted from macrophages using the Monarch Total RNA Miniprep kit (VWR, UK) as per the manufacturer's instructions omitting the proteinase K step of the protocol. Lysis buffer was added at a volume of 300 μl to each well to lyse the macrophages. The lysate was pipetted multiple times to ensure maximum cell lysis and then transferred to a Monarch gDNA removal column. Samples were centrifuged at 16,000 x*g* for 30 s to remove gDNA. The flow through was combined with an equal volume of ethanol (>95 %) and then applied to a Monarch RNA purification column. DNA was digested using DNase I as per manufacturer's recommendations. RNA was eluted in 60 μl of nuclease-free water. The eluted RNA was passed through the column again to maximise RNA recovery. The concentrations of RNA extracted from all samples were measured using a Nanodrop 1000 (Thermo Fisher Scientific, UK) by measuring the absorbance at 260 nm ($A_{260}$) and 280 nm ($A_{280}$). RNA purity was assessed using the $A_{260}/A_{280}$ ratio. Samples with $A_{260}/A_{280}$ of ≥2 were deemed pure.

#### 2.10.2. Reverse transcription-quantitative polymerase chain reaction (RT-qPCR)

One μg of total RNA from each sample was converted into cDNA using a QuantiTect Reverse Transcription kit (Qiagen, UK). Briefly, genomic DNA was removed from the total RNA samples using gDNA Wipeout buffer and heating to 42 °C for 2 min. The treated RNA was then reverse transcribed into cDNA following the manufacturer's instructions. For RT-qPCR, cDNA was diluted 1:5 with RNAse-free water. Quantitative PCR was performed using TaqMan gene expression assays using a two-step RT-qPCR protocol: initial denaturation for 3 min at 95 °C, followed by 40 cycles of denaturation for 10 s at 95 °C and annealing/elongation for 30 s at 60 °C. All reactions were performed in triplicate using pre-designed primers (Applied Biosystems, Thermofisher, UK) using VIC-labelled reference probe *β2-microglobulin* probe (Hs00187842_m1) serving as reference gene and FAM-labelled target probes for: *CD80* (Hs01045161_m1), *CD86* (Hs01567026_m1), *CD163* (Hs00174705_m1), *CD206* (Hs07288635_g1), *IL-1β* (Hs01555410_m1), *IL-6* (Hs00174131_m1), *IL-10* (Hs00961622_m1), *IL-13* (Hs00174379_m1), *CCR7* (Hs01013469_m1), *TNF-α* (Dr03126850_m1)

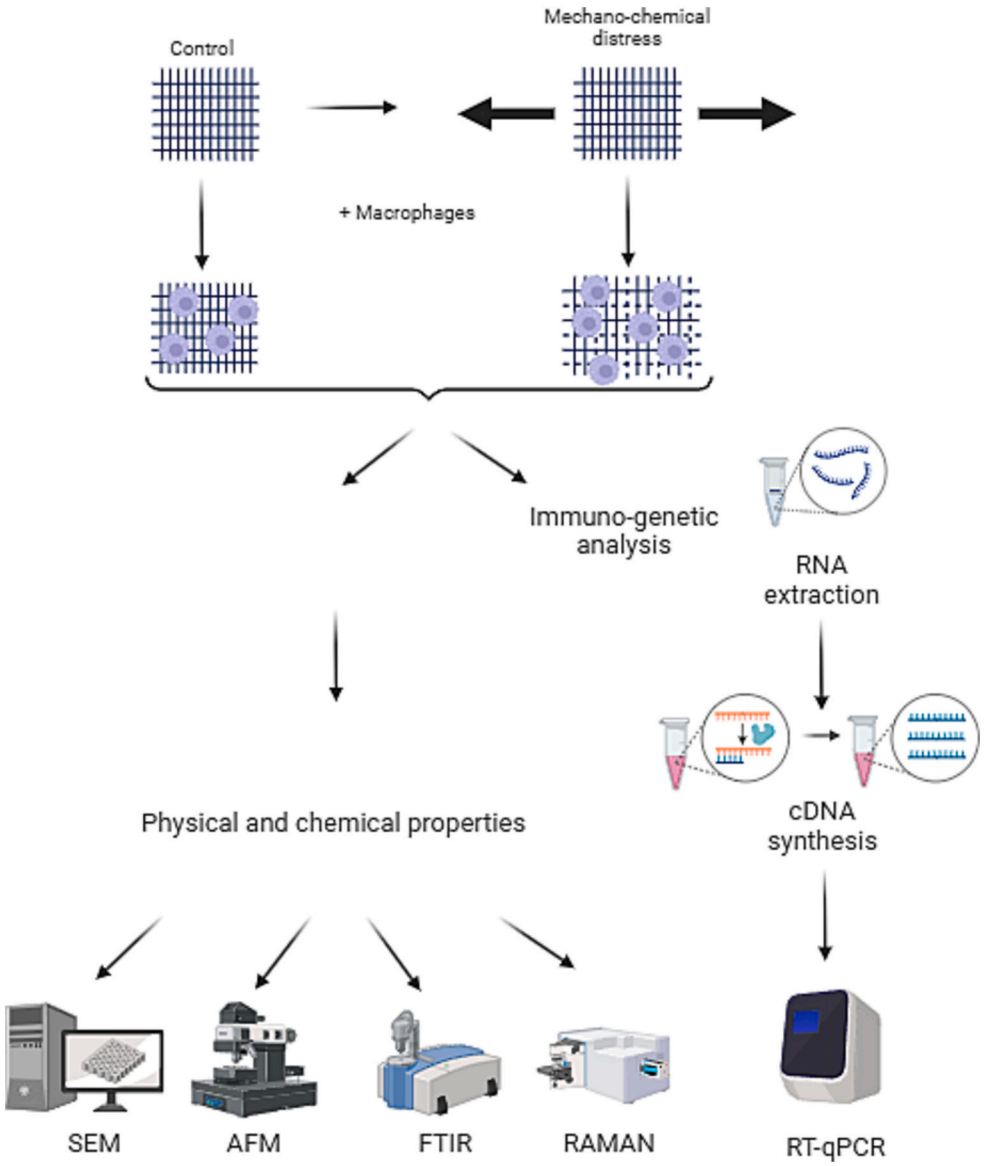


**Fig. 1.** Schematic diagram outlining the experimental techniques used to analyse PP surgical mesh, including physical, chemical and immunogenetic analysis. PP surgical mesh was taken and either used directly or subjected to mechanochemical distress for 72 h. Macrophages were then added to samples of control or mechanochemically distressed PP mesh and cultured for 7 days. All samples of mesh (with and without cells) were subjected to Scanning Electron Microscope (SEM), Atomic Force Microscope (AFM), Fourier-transform infrared spectroscopy (FTIR) and RAMAN spectroscopy. RNA was extracted from macrophages cultured on control or mechanochemically distressed PP surgical mesh. After cDNA synthesis, quantitative PCR (RT-qPCR) analysis was carried out to distinguish the immunogenic response of macrophages to the PP surgical mesh.

and *TGF-β1* (Hs00998133_m1). All RT-qPCR reactions were performed using a QiaQuant 96 thermal cycler (Qiagen, UK). Fluorescence was measured at 518 nm (FAM) for genes of interest and 554 nm (VIC) for the reference gene at each cycle. Threshold cycle (Ct) values were obtained by recording cycles at which 0.04 fluorescence units were reached. Relative gene expression of the gene of interest compared to the reference gene *β-2-microglobulin* (*B2M*) was calculated using the $2^{-\Delta\Delta Ct}$ method where $\Delta\Delta Ct = \Delta Ct$ sample $- \Delta Ct$ reference control.

### 2.11. Statistical analysis

RT-qPCR analysis was performed on three independent experiments with each experiment carried out in triplicate. The mean and standard deviation (SD) were calculated from the three independent repeats, where the mean of the RT-qPCR triplicates were used for each biological repeat. To compare the mean values, an unpaired Student's *t*-test was performed using Graphpad Prism v9.5 software and statistical significance was determined when: *, $P \leq 0.05$; **, $P \leq 0.01$; ***, $P \leq 0.001$ and ****, $p < 0.0001$ compared to the control. Fold change values for each gene were calculated by averaging samples compared to M-TCP and grouped column graphs generated as log2(Value/M-TCP) with SD.

## 3. Results

### 3.1. Assessment of surface morphology and topography using SEM/AFM

Surgical polypropylene (PP) mesh was either used straight from the packaging or subjected to mechanochemical distress. Fully differentiated monocyte-derived macrophages were cultured on control and mechanochemically distressed mesh. Samples from each of the four groups were analysed using low voltage (LV)-SEM. It is important to note that control mesh itself has some surface markings. Despite the

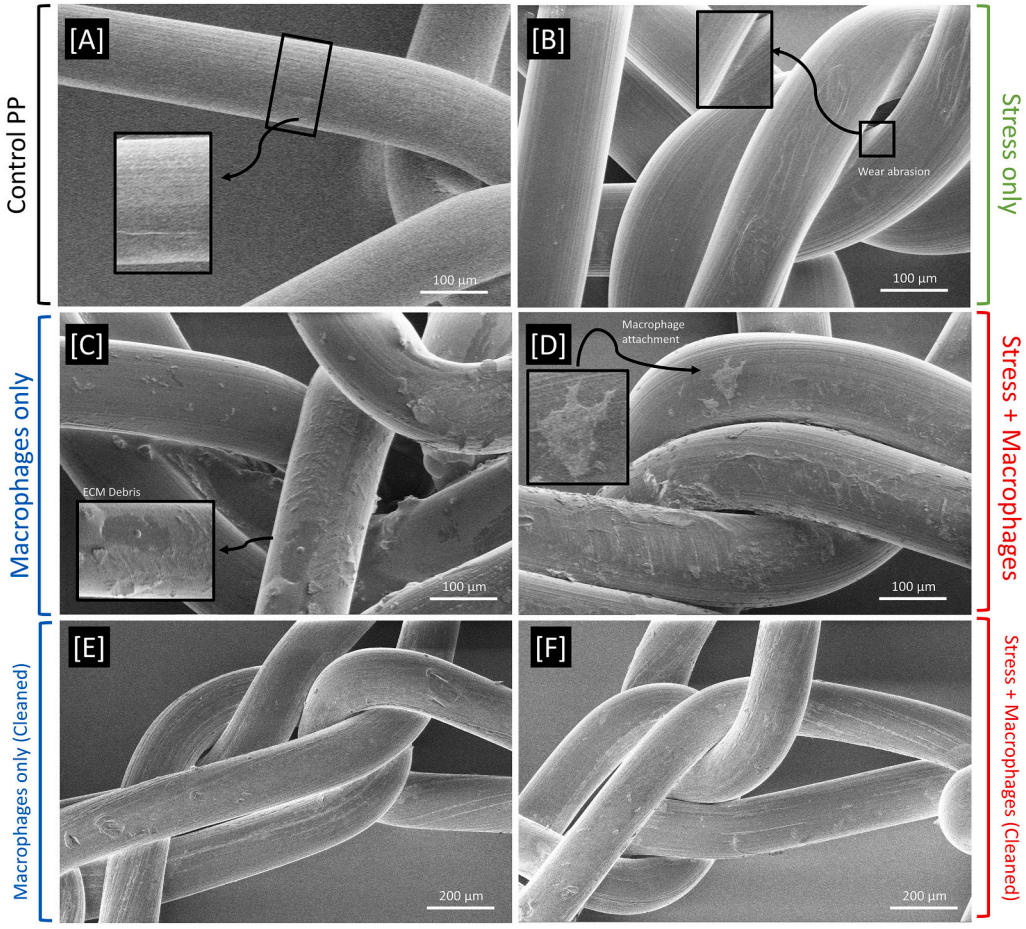


**Fig. 2.** SEM images of control PP (A), mechanochemically distressed PP (B), control PP + macrophages (C) and mechanochemically distressed PP + macrophages (D). Control PP + macrophages after cleaning (E) and mechanochemically distressed PP + macrophages after cleaning (F).

control mesh undergoing no treatment, surface markings were present on the fibres due to the extrusion of the fibres during fabrication (Fig. 2A). As a result of applying mechanochemical stress (Fig. 2B) areas of plastic deformation and abrasion became visible in addition to the extrusion markings that were present in the control fibres. Furthermore, what appear to be loose particles were also notable in areas of abrasion resulting from mechanochemical distress. These particles, despite being low in number, are an example of mechanical wear debris.

When macrophages were added to control (Fig. 2C) or distressed PP (Fig. 2D), cellular debris was observed and fragments of the ECM were observed adhered to the fibres. To more clearly observe the changes to fibre surfaces the samples were washed with $dH_2O$ and then imaged (Fig. 2E and F). The main difference observed between control mesh with macrophages (Fig. 2C and E) and distressed mesh with macrophages (Fig. 2D and F) is that wear abrasion was observed in the latter. Comparing control mesh (Fig. 2A) and mechanochemically distressed PP with macrophages (Fig. 2D and F) manifold differences were observed. Areas of surface abrasion and surface cracking, which are perpendicular to the fibres, can be observed in the bottom left of the image (Fig. 2D). Surface degradation can also be observed as a result of macrophage culture on the PP. Micron-sized particles were also observed on stressed mesh with macrophages. These are highlighted in Supplementary Fig. 1 and size distribution was measured (Supplementary Fig. 2).

To better understand the nanoscale surface topography, AFM images were obtained. The control PP (Fig. 3A) and mechanochemically distressed PP samples (Fig. 3B) showed similar differences in surface topography as observed in the SEM analysis. Comparable wear abrasion with consistent characteristics were present on the mechanochemically distressed samples (Fig. 3B). The mechanochemically distressed sample topography differed from the control sample with respect to the amount of nano-micron scale particles present. An example of this is shown in Fig. 3B as surface friction has created what appears to be two discernible wear abrasion marks on the surface of the fibre. Debris particles were mostly observed surrounding these structures. It is conceivable that ECM and debris from produced from macrophages could contribute to such topographic alterations, however LV-SEM images presented after cleaning show that surface changes were still present when ECM/debris was removed. Fig. 3C, showing control PP with macrophages, captured a macrophage still attached to the fibre surface. Surrounding this macrophage there appeared to be the remains of ECM. The fibre surface not covered with ECM residue consisted of longitudinally aligned fabrication marks with minor surface cracks (Fig. 3C) more comparable to that of the control PP. The greatest extent of surface fragmentation and particle production was observed in mechanochemically distressed PP with macrophage attachment (Fig. 3D). The combination of applied mechanochemical distress and macrophage attachment also created notably larger surface cracks.

### 3.2. *Identifying alterations in bulk mechanical properties*

Using a tensiometer the tensile properties of all treated PP meshes were obtained and comparisons to control PP made. Typical stress strain curves for each group are displayed in Fig. 4A alongside the calculated Young's modulus (Fig. 4B). PP meshes which had undergone dynamic distention, with or without the inclusion of macrophages, showed a significant difference in their stress-stress curves and Young's modulus.

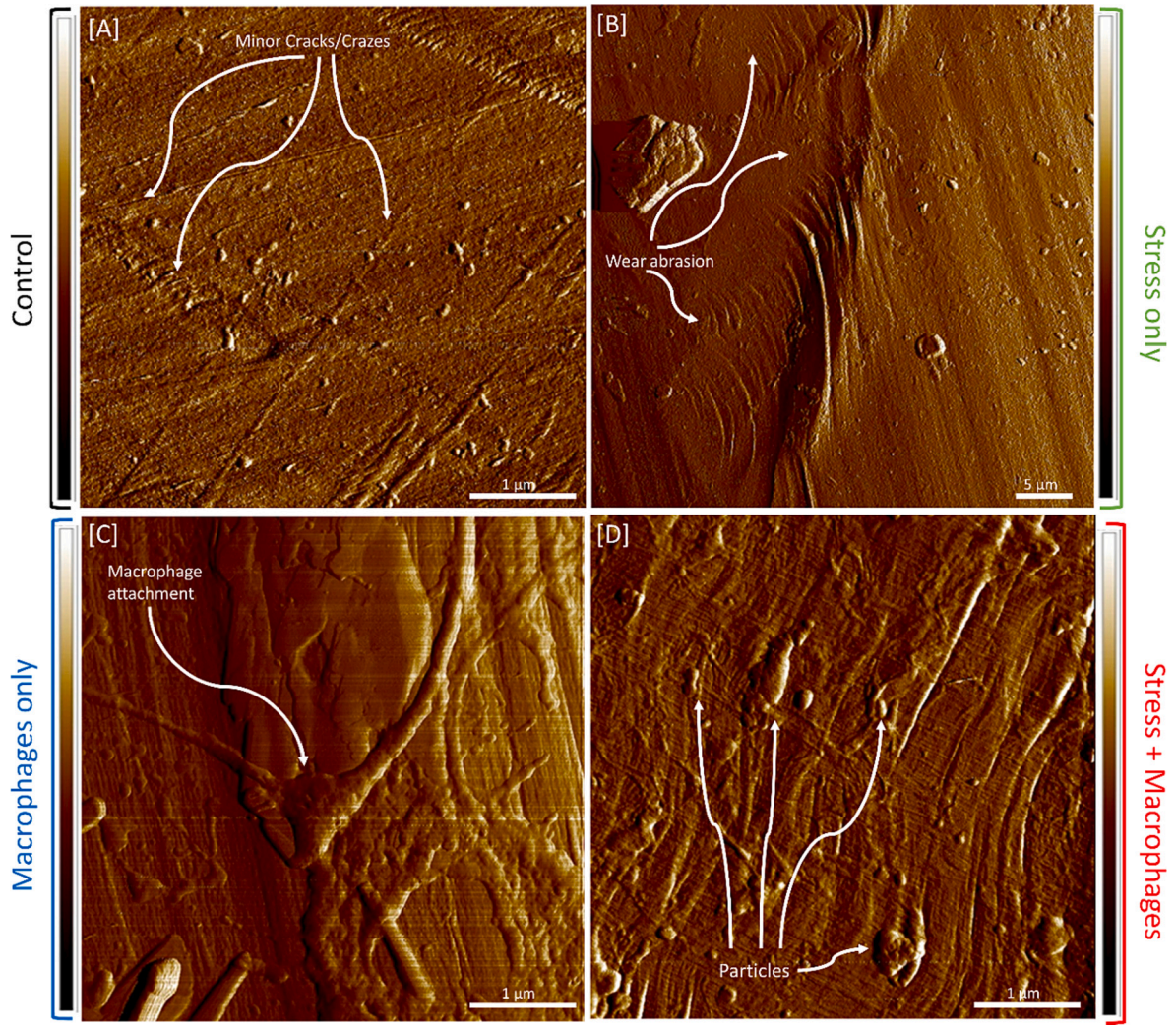


**Fig. 3.** A – D presents AFM peak height images (6 µm - 0 µm height scale) of control PP (A), mechanochemically distressed PP (B), control PP + macrophages (C) and mechanochemically distressed PP + macrophages (D).

This result is consistent with previously published studies which have shown the fibre stiffening effect of repeated dynamic distention of PP mesh [4,5]. Macrophage attachment alone did not cause a significant impact on mechanical properties of the bulk mesh fibres. However, a notable trend of fibre stiffening was identified from mesh cultured with macrophages compared to that of control PP.

### 3.3. Quantification of sub-surface chemistry by ATR-FTIR and Raman spectroscopy

To obtain a measure of oxidation for all PP meshes, ATR-FTIR was performed. Fig. 5 presents the ATR-FTIR spectra obtained from a control PP mesh sample and all test samples. FTIR spectra of control (Fig. 5, blue spectrum) and stress only (Fig. 5, green spectrum) display similar FTIR peaks, which are expected from PP [32,33]. Samples which had been exposed to macrophages (Fig. 5, red (mechanical stress + macrophages) and blue spectra (macrophages only)) showed pronounced carbonyl C═O (expected range: 1750–1500 $cm^{-1}$) and C—O peak at 1056 (expected range 1100–1000 $cm^{-1}$) bands compared to that of both the control and stress only samples. Previously studies have associated the presence of carbonyl peaks with the oxidative degradation of PP mesh both *in vitro* and *in vivo* [5,34–36]. To further verify these findings EDX was performed on all samples (Supplementary Fig. 4). EDX has previously been applied to identify oxidation of PP explanted from patients [35]. Peaks related to carbon and oxygen were present in all samples, however the ratio of oxygen to carbon notably increased for both mesh samples cultured with macrophages. EDX also provided evidence, through the lack of identifiable nitrogen, that the process of washing the samples with $dH_20$ prior to the quantification of sub-surface chemistry was sufficient to remove any residual cell contamination.

In order to identify the impact of the test conditions on the PP backbone structures, Raman spectroscopy was performed (Fig. 6). Supplementary Table 1 contains the vibrational assignment for Raman bands of PP, previously published in detail [37]. It is worth noting that the spectrum (Fig. 6, black spectrum) obtained for the control PP mesh is consistent with previously published data [38]. Changes in the ratios of 1150/1168, 972/995 and 808/841 $cm^{-1}$ bands were observed in response to mechanochemical distress being applied to the polymer fibres (Fig. 6, green and red spectra). No notable differences were seen between spectra collected from control mesh (Fig. 6, black spectrum) or control mesh with macrophages (Fig. 6, blue spectrum). There also did not appear to be any differences between spectra collected from mechanochemically distressed mesh with (Fig. 6, red spectrum) or without macrophages (Fig. 6, green spectrum).

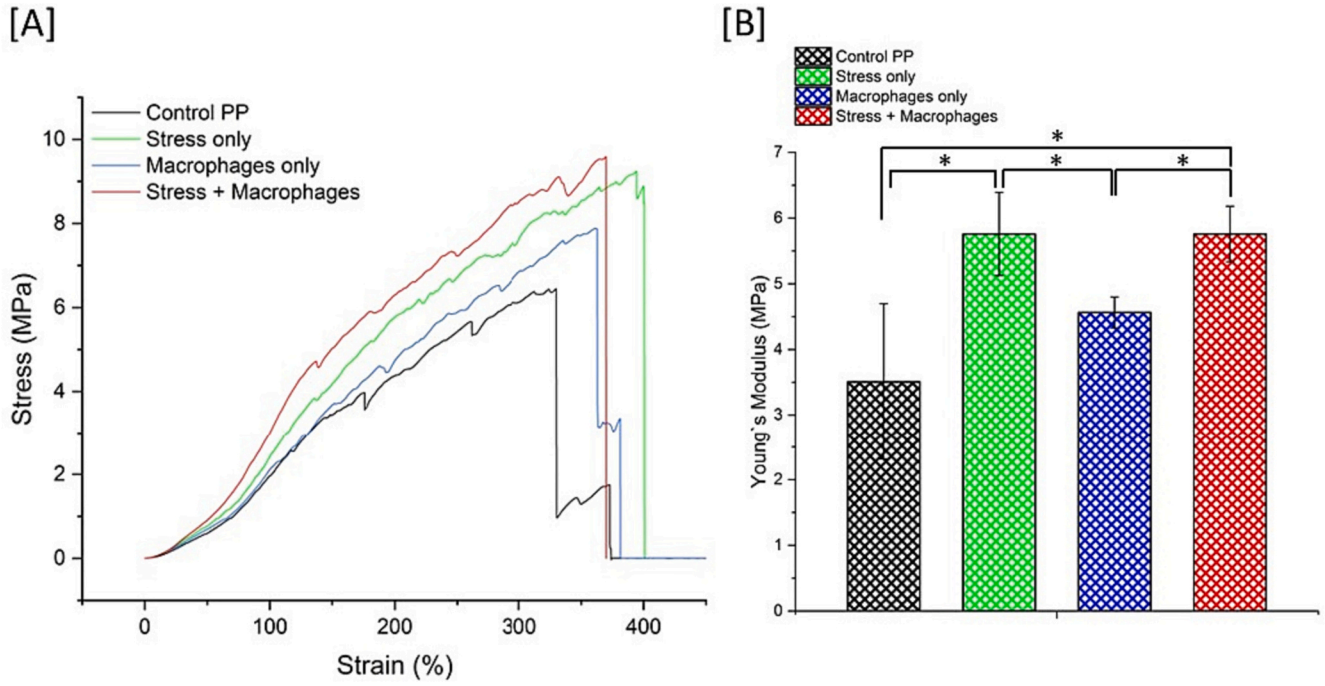


**Fig. 4.** (A) Stress-strain curves of PP mesh samples ($n = 3$). (B) Graph presenting the Young's modulus of PP meshes after treatment (n = 3) (*$p < 0.05$ significance).

### *3.4. Macrophage responses to control and mechanochemically distressed PP mesh*

RT-qPCR was used to assess the gene expression profile of pro-inflammatory (*TNF-α*, *IL-6*, *IL1-β*, *CCR7*) and pro-fibrotic (*TGF-β*, *IL10*, *IL13*) markers as well as cell surface markers (*CD80, CD86, CD163, CD206*) by macrophages in response to control and mechanochemically distressed PP mesh. In comparison to macrophages cultured on tissue culture plastic (M-TCP) cell surface markers *CD80* and *CD86* (M1 phenotype) and *CD206* (M2 phenotype) were up-regulated, whereas CD163 (M2) was down-regulated. There were significant differences between gene expression for all surface markers except *CD86* (M1). Macrophages exposed to control PP for 7 days down-regulated all pro-fibrotic markers and 2 pro-inflammatory markers (*IL-1*β and *IL-6*). The other 2 pro-inflammatory markers were slightly (*TNF-α*) or >2-fold (*CCR7*) up-regulated (Fig. 7, blue, hatched bars). In contrast, macrophages exposed to mechanochemically distressed PP for 7 days up-regulated all pro-fibrotic and pro-inflammatory markers except *CCR7*, giving a mixed pro-inflammatory and pro-fibrotic response (Fig. 7, red bars). The most significantly up-regulated (fold change >1.5) genes were *IL1-β* (pro-inflammatory) and *TGF-β1*, *IL-10*, and *IL-13* (pro-fibrotic; all $p < 0.001$). There was no difference in the levels of *TNF-α* between the two conditions.

## 4. Discussion

### *4.1. Novel insights and significance*

Although there have been decades of designing biomaterials appropriate for the clinical environment, when adverse reactions occur we suggest there is a need for better *in vitro* investigative tools to improve our knowledge of how materials might respond *in vivo*. This approach is aimed at reducing the number of animal experiments and initial safety studies in humans, generating improved confidence in selecting the most appropriate biomaterials to take forward to clinical evaluation.

Specifically, through analysing differential gene expression of macrophages cultured on PP mesh we have gained a better understanding of how macrophages respond to a biomaterial, described in detail in Sections 4.2–4.4, but summarised as follows:

1) The use of mechanical distension in combination with mild oxidation as opposed to static conditions have allowed us to observe altered gene expression from macrophages cultured on PP mesh.
2) In the absence of external stimuli, the presence of macrophages alone will modify the PP surface by oxidising it.
3) Culturing macrophages on mechanochemically distressed PP results in formation of particles.
4) Culturing macrophages on the surface of the PP surgical mesh promotes oxidation. This surface oxidation was observed using ATR-FTIR and EDX only after macrophages were cultured on the mesh.
5) The application of mechanochemical distress (the ability to break and make chemical bonds) causes helical chain defects in the PP polymer backbone observed by changes in the Raman signature as well as physical cracking and crazing of the fibres. Macrophages were not observed to cause helical chain defects in isolation.

Based on these observations it is hypothesised that when macrophages are grown on the surface of PP mesh that has previously been exposed to mechanochemical distress, they oxidise the surface, as well as act on cracks that have been formed to further oxidise deeper PP layers. Macrophages responded to this combination of deeper oxidation and polymer backbone breakage by upregulating expression of pro-inflammatory and pro-fibrotic genes. In contrast, macrophages responded to control mesh by downregulating pro-fibrotic and pro-inflammatory genes. These data show that mechanochemical distress causes changes to the PP that elicits a strong inflammatory and fibrotic reaction from macrophages cultured on it. In comparison, the macrophage response to PP without mechanochemical distress is altered. Thus this novel approach has allowed us to propose that there is an interaction between the material and macrophages as summarised in the cycle in Fig. 8B. This cycle of cellular response: changing the mesh characteristics changes the cellular response, may continue during the implantation lifecycle of the mesh. The above hypothesis and proposed cycle is based on considering the interplay of changes in physical appearance of the surface and bulk chemical changes and their combined effect on macrophage gene expression.

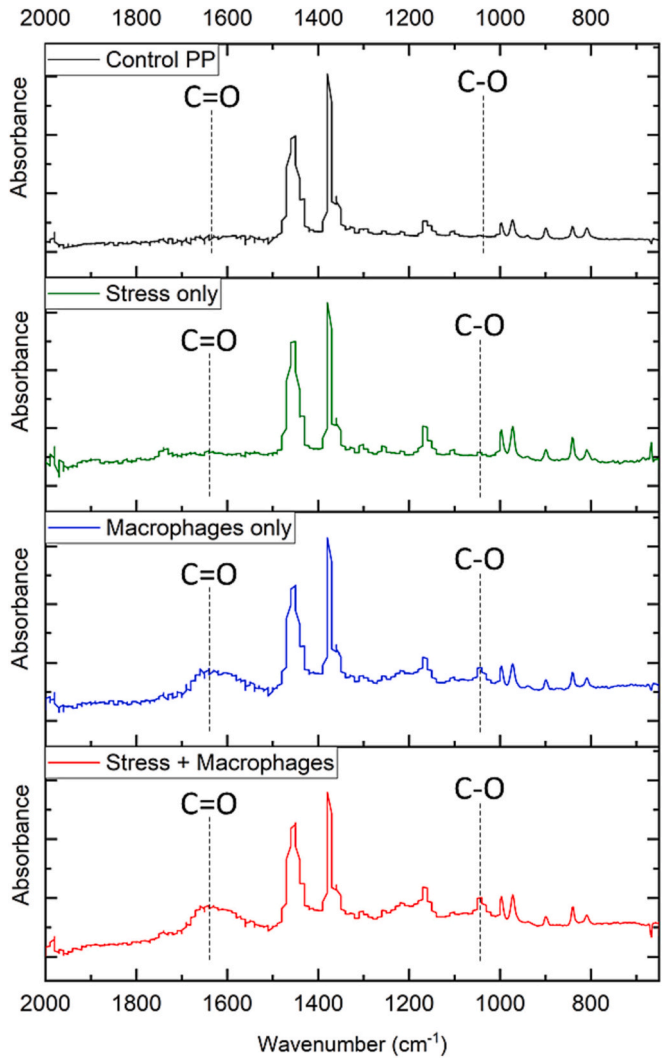


**Fig. 5.** ATR – FTIR spectra of control PP (black spectrum), mechanochemically distressed PP (green spectrum), control PP + macrophages (blue spectrum) and mechanochemically distressed PP + macrophages (red spectrum).

### 4.2. Physical appearance/surface roughness/macrophage response

It has been long established that an inflammatory environment can lead to surface changes in a biomaterial [14,15]. It was expected that PP degradation, as commonly observed in many plastics, would first occur at the polymer surface. Therefore, surface analysis is imperative for the study of polymer degradation [39]. Both SEM and AFM were used to examine PP mesh fibres, where nanoscale crazes/cracks introduced during the fabrication process were observed. These markings are often found longitudinally and are considered to be due to the oxidation and mechanical stress applied in the fabrication of the mesh knit structures.

In this study the application of mechanochemical distress and cellular attachment both imparted different visually identifiable defects on the surface of PP fibres. Both SEM and AFM imaging revealed crazing, cracking and particle production on the surface of mechanochemically distressed fibres compared to that of control PP mesh. Crazes form as a precursor to a larger crack forming process as creep load is applied to the fibres [40]. When mechanochemical stress was applied to the PP fibres craze-induced defects greatly increased in both size and abundance. The application of mechanical stress also led to fibre wear abrasion, as fibres around knot sites are in close proximity thus causing friction through fibre-fibre interactions. Such abrasion between fibres results in the production of particles, which are notable on the surface of fibres post-mechanochemical distress. These particles are often microns in diameter and are likely to generate an inflammatory response [41–43].

However, for PP samples whether or not they were subject to mechanochemical distress, it was notable that the inclusion of macrophages impacted on the surface structures and fragments present. We suggest that the imperfections produced in the fabrication of the mesh may act as a trigger point for both oxidative and mechanical stress-initiated degradation. Indeed, after the input of mechanochemical distress and with subsequent exposure to macrophages the cracks in the PP mesh were observed to be more extensive and larger in size. Macrophages have abundant filopodia that actively probe their environment, acting as cellular tentacles to increase efficiency of pathogenic uptake [44], as well as to aid adhesion to substrates as part of the foreign body response [45]. These filopodia could be used to probe the fibre surface, find the pre-existing surface defects and act to increase them. It has been shown that adherent macrophages can exert sufficient force to break polymer chains leading to polymer degradation and, ultimately, biomaterial failure [13,46,47]. These findings taken in combination again support the argument that mechanical distension should be applied during *in vitro* testing to better replicate the *in vivo* environment.

With respect to the appearance of the PP fibres surface post-macrophage attachment, clear cell debris was observed. This material appears to be ECM components or debris remaining from previously attached macrophages, which is not surprising as they are known to express virtually all known collagen and collagen-related mRNAs as well as secreting type VI collagen [48]. By cleaning the fibre surface it is notable that the inclusion of macrophages, both alone and in combination with mechanochemical distress, impacts on the surface structures. It has been postulated previously that oxidative stress, in this instance from reactive oxygen species produced by macrophages, is responsible for chemically etching away at the surface [13].

### 4.3. Bulk chemical and mechanical changes

It has previously been established that Raman spectroscopy can be used to characterise PP surgical mesh [38,49]. The bands found at 808, 841, 972, 995, 1168 $cm^{-1}$ are related to the helical chain structure of PP. Variations within these band ratios revealed a notable helical structural change in response to mechanochemical distress being applied to the polymer fibres. Analysis of the Raman band ratio of 808 $cm^{-1}$ and 841 $cm^{-1}$ (Supplementary Fig. 3) has been previously shown to relate to conformational states of helical chains. Therefore, the relative ratio of the two bands has been previously used to estimate the degree of crystallinity and helical chain defects in PP [49–51]. 808 $cm^{-1}$ is associated with helical chains within crystals (r(CH3) and backbone stretching $\nu$(C—C)), whilst 841 $cm^{-1}$ is associated with shorter chains in helical conformation [49]. Fragmentation reactions leading to lower molecular weight chains are common in PP degradation [52]. This is often attained through free radical reactions resulting in molecular chain scission [53]. An increase in the 841 $cm^{-1}$ band suggests that PP has fragmented to give shorter chains showing helical chain defects.

Both control PP and control PP + macrophages exhibited a similar 808/841 $cm^{-1}$ ratio. With no clear increase present in the 841 $cm^{-1}$ band it can be assumed that the addition of macrophages to control PP did not cause any notable helical chain defects. However, both mechanochemical distress alone and mechanochemical stress + macrophages did show a shift in the 808/841 $cm^{-1}$ ratio with the growth of the 841 $cm^{-1}$ band showing helical chain defects. Our laboratory has previously shown that dynamic distention of PP mesh for just 3 days causes irreversible distortion and failure in the mesh structure [4]. Therefore, this result is not unexpected as alterations in the molecular structure of PP are consistent with changes in bulk mechanical properties obtained in this study.

ATR-FTIR and EDX data obtained indicated that oxidation had occurred on PP fibres after cellular attachment. It has long been established that environmental stresses, both oxidative and mechanical, can

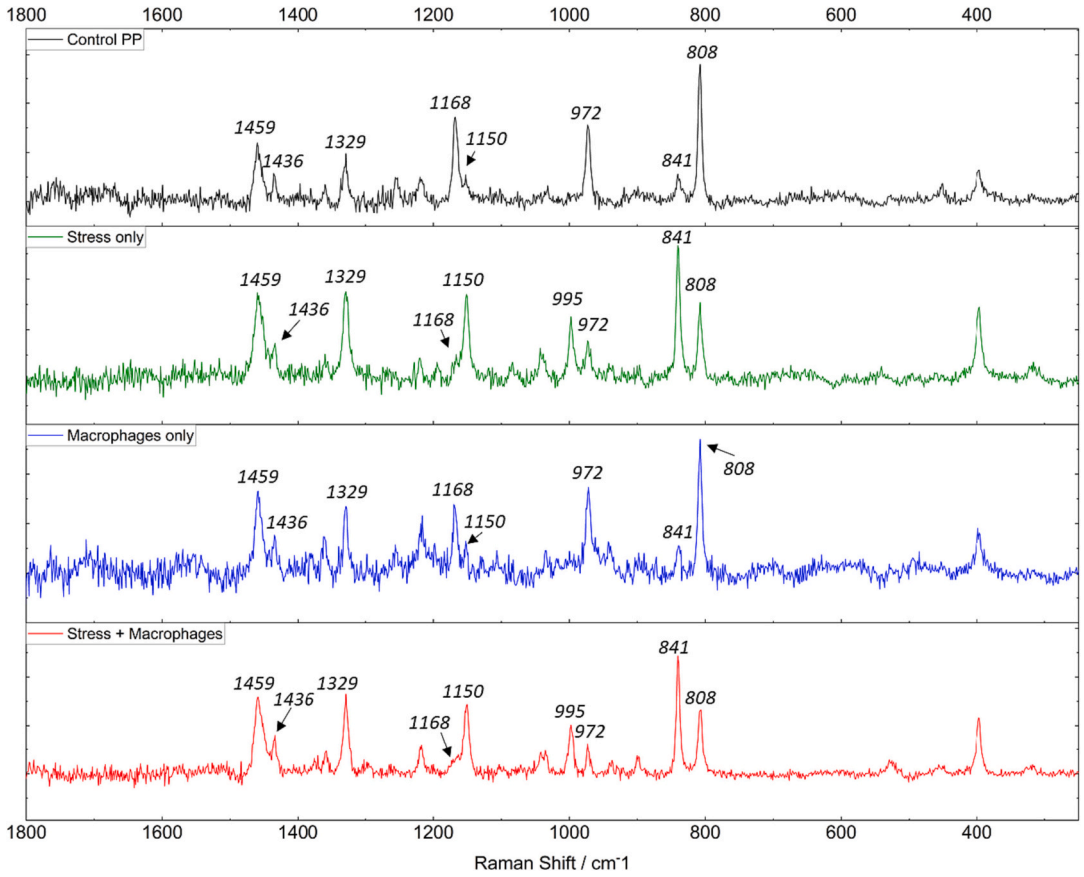


**Fig. 6.** Raman spectra of control PP (black spectrum), mechanochemically distressed PP (green spectrum), control PP + macrophages (blue spectrum) and mechanochemically distressed PP + macrophages (red spectrum).

lead to the formation of PP radicals [35,54–56]. In the process of oxidation of PP these free radicals, which react in the presence of oxygen [35], will trigger the formation of new functional groups, especially carbonyl and hydroperoxides [35,57]. As both carbonyl and hydroxyl groups were observed using ATR-FTIR in the presence of macrophages it can be stated that oxidation of PP is confirmed in these samples. Previous studies have described the route to oxidation of PP in depth and proposed an *in vivo* degradation pathway [33,58].

Of additional interest, it can be seen that mechanochemical distress increases the formation of both carbonyl and hydroxyl groups compared to the effect of macrophages alone. This result is not unexpected as it is likely that the creation of surface cracking (as shown in Fig. 2) can facilitate oxidation by increasing the surface area exposed to an oxidising agent. The oxidising agents in this study were both preconditioning with $H_2O_2$ treatment and reactive oxygen species directly released from macrophages. It should be noted that surgical PP mesh used clinically for pelvic organ prolapse and stress urinary incontinence reconstruction should be designed to withstand both the oxidative and mechanical stresses of lifelong implantation.

### 4.4. Changes to macrophage gene expression

After 7 days of culture on both the control and mechanochemically distressed mesh samples, macrophages exhibited similar gene expression patterns for cell surface markers. Although there were significant differences between groups, the overall pattern observed was the same. Both M1 markers (*CD80*, *CD86*) were slightly up-regulated, *CD163* (M2 marker) was down-regulated and *CD206* (M2 marker) was highly up-regulated (over 2-fold change compared to macrophages grown on TCP). The expression pattern seen is indicative of a mixed phenotype (similar to that shown in human patients with interstitial lung disease [59]). The evidence for a mixed phenotype is further supported by the expression profile observed for pro-inflammatory and pro-fibrotic genes, which is also clearly divergent between the two groups. The macrophages on the control PP mesh up-regulated the inflammatory genes *TNF-α* and *CCR7*, all other genes were down-regulated. Macrophages cultured on the mechanochemically distressed mesh however, exhibited a strong inflammatory and fibrotic response as seen by up-regulation of the potent inflammatory and fibrotic markers *IL1-β* and *TGF-β* respectively. This mixed phenotype has been observed previously, and is thought to be unique to macrophage activation by biomaterials [13,60].

One of the key pathways that initiates and drives fibrosis in the human body is the TGF-β pathway. TGF-β is a potent pro-fibrotic cytokine implicated in various organ-based as well as biomaterial-induced fibrosis [60,61]. Once produced by macrophages TGF-β attaches to receptors in the cell membrane and is transported to the nucleus where it promotes transcription of genes encoding pro-fibrotic proteins. *In vivo* these proteins promote differentiation of fibroblasts into myofibroblasts which are one of the key effector cells in biomaterial-induced fibrosis [20]. Myofibroblasts then lay down collagen around the implant to form a capsule in an attempt to separate it from the rest of the body. Macrophages fuse and become foreign body giant cells, adding to the fibrotic capsule.

Macrophages cultured on mechanochemically distressed surgical mesh exhibited a strong pro-fibrotic response as exemplified by up-regulation of the *TGF-β* gene in these cells. All profibrotic genes investigated were upregulated as well as *TNF-α*, *IL-1β* and *IL-6*. Although described as pro-inflammatory cytokines TNF-α, IL-1β and IL-6 have a pleiotropic effect and can promote fibrosis *via* trans-signalling of the TGF-β pathway in fibroblasts *in vivo* [62,63]. The inflammatory genes *TNF-α*, *IL-6* and *IL1-β* are all implicated in acute inflammation but can also augment a fibrotic response [60,62,64]. The pro-fibrotic activity of

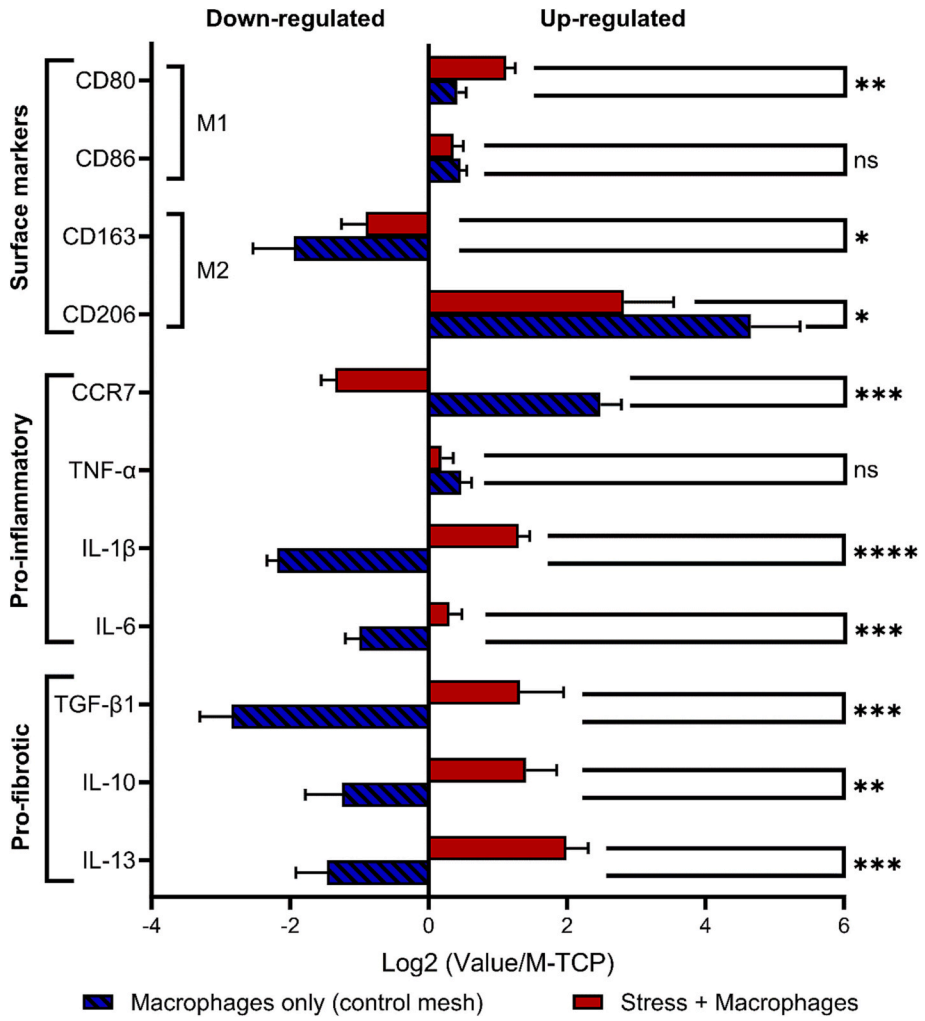


**Fig. 7.** Expression of selected genes in macrophages exposed to control PP + macrophages (blue bars) or mechanochemically distressed PP + macrophages (red bars). *$p < 0.05$, **$p < 0.01$, ***p < 0.001 and ****$p < 0.0001$. Data represent mean ± SD of three independent biological experiments, with each experiment carried out in triplicate ($N = 3$, $n = 3$).

IL-6 is well known in fibrotic diseases like systemic sclerosis, cardiac and renal fibrosis [65]. Similarly, the pro-inflammatory cytokines TNF-α and IL1-β have a pro-fibrotic effect as evidenced by their role in fibrotic diseases in different organs [64,66,67]. The pro-fibrotic cytokine IL-13 stimulates the production of TGF-β1 especially in combination with TNF-α. IL-10 is an anti-inflammatory cytokine with a pleiotropic effect that is concentration dependent. At normal levels, it exhibits an anti-inflammatory effect but when over-expressed, it can promote fibrosis as demonstrated by the increased TGF-β expression in the lungs of IL-10 transgenic mice [68].

*In vivo* data from animal studies and analysis of mesh explanted from the pelvic floor of symptomatic patients also highlights the role of IL-10 in fibrosis. In a study by Brown et al., three different polypropylene meshes of different weight and porosities were implanted into Rhesus macques [69]. These were explanted 12 weeks later and the macrophage response studied. Histologic evaluation revealed a pro-fibrotic response in the lighter, more porous meshes with significantly raised IL-10 levels compared to a pro-inflammatory response in the heavier, less porous mesh. Similarly, Nolfi et al. showed raised inflammatory and fibrotic cytokines in mesh-tissue complexes excised from symptomatic patients up to 36 months post-implantation [19]. Interestingly, levels of IL-10 were raised significantly in the patient group complaining of pain, whereas the inflammatory cytokine MMP-9 was raised in the group with mesh extruding out of their body. MMP-9 is a proteolytic enzyme that can cause extracellular matrix degradation [70]. It can also activate certain growth factors, including TGF-β [71]. Thus both inflammatory and fibrotic pathways are active in patients where mesh is subjected to mechanochemical distress in their bodies, years after implantation.

The pro-inflammatory and pro-fibrotic molecular signature of the macrophages in response to the mechanochemically distressed mesh clearly demonstrates that *in vitro* as the PP mesh changes, the macrophage response changes with it. To compare this to the clinical setting, freshly implanted mesh (denoted control mesh in this study) provokes an inflammatory reaction in macrophages immediately present. This inflammatory reaction activates fibroblasts to differentiate into myofibroblasts, lay down collagen and form a capsule. The encapsulated mesh is then subject to mechanical as well as oxidative stresses in the pelvic floor. We have shown that the action of macrophages and mechanochemical distress causes chemical and physical changes to the mesh. Macrophages then respond to these changes by up-regulating fibrotic genes and expressing genes for cytokines that will exacerbate the fibrotic response. Mechanochemical stress may also lead to breakage of the capsule in the body and exposure of the mesh which would restart the inflammatory process. This leads to a persistent inflammatory picture which would promote fibrosis. The cellular response of the macrophages to the stressed mesh cohort demonstrates this. This cycle, illustrated in Fig. 7B, may continue for the lifetime of the biomaterial and could lead to a biomaterial being poorly tolerated.

Therefore, there was expression of both pro-inflammatory and pro-fibrotic genes in macrophages cultured on mechanochemically

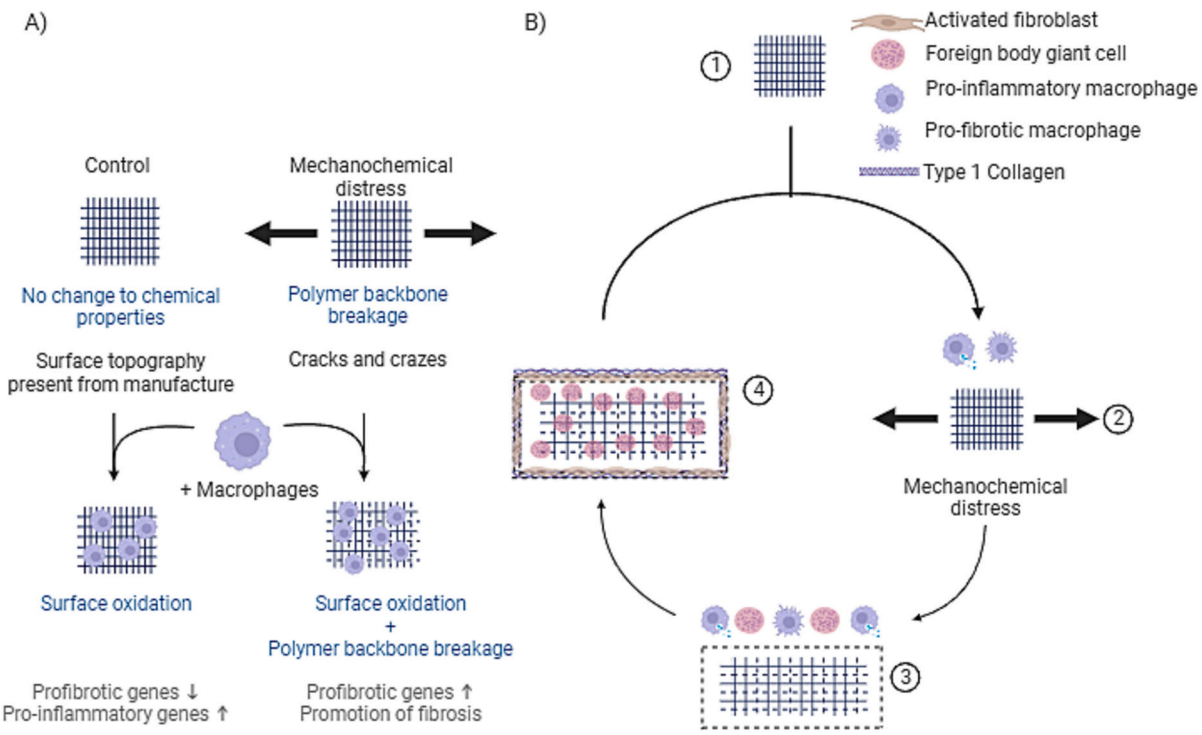


**Fig. 8.** (A) Schematic summary of the changes seen in the physical and chemical properties (blue text) of the PP surgical mesh and effect on immuno-genetic fingerprint of the macrophages (grey text). (B) Schematic representation of the proposed interactions between cells and polypropylene mesh during its lifecycle after implantation *in vivo*. (1) Polypropylene mesh immediately after implantation with an inflammatory response from macrophages. (2) PP mesh subjected to mechanical distension in the body as well as oxidative stress from the macrophages leading to breakage of polymer backbone. (3) Macrophages change to a pro-fibrotic phenotype in response to changed PP mesh (4) Formation of a collagen type 1 capsule, foreign body giant cells and activated fibroblasts which cause contraction and further change in the mesh. This cycle of cellular response: changing the mesh characteristics changes the cellular response, may continue during the implantation lifecycle of the mesh which can lead to tissue driven contraction of the mesh and erosion through tissues.

distressed mesh. This response could signify an early shift towards fibrosis. A prolonged/extended inflammation phase is thought to influence a more fibrotic or pathological wound healing response *in vivo* [72].

### 4.5. Narrowing the gap to more effective in vitro testing

The current study demonstrates activation of macrophages *in vitro* in response to mechanochemically distressed PP surgical mesh. As macrophages are only one cell type in the immunologic cascade the findings are necessarily restricted. Including fibroblasts in this model would allow the possible fibrotic response initiated by macrophage signalling to be observed. Ideally studying the responses of macrophages and fibroblasts *in vivo* to surgical mesh would be informative but there are real difficulties in trying to access relevant clinical samples from patients suffering from adverse effects to these materials. Accordingly, we have obtained tissues from animals implanted with these mesh materials and hope to report on these soon. All of this should help progress our understanding of the biomaterial-induced fibrosis observed in animal models and patients.

The gene panel currently used has been identified from the literature. Examining macrophage and fibroblast gene expression and cytokine release *in vivo* may allow a more pertinent panel to be established and used *in vitro*. The observed response of macrophages to the mechanochemically distressed mesh could be due to any, all or a combination of the following factors; oxidation, particles, topography, cracks, and material. Further studies are required to investigate this further. The current data demonstrates the need to further develop useful *in vitro* models allowing investigation of materials under mechanochemical stress and cellular interrogation.

## 5. Conclusions

Our study presents for the first time a test model that combines *in vitro* provocation of a biomaterial (mechanical distension + $H_2O_2$) with macrophage exposure. Changes to material properties were detected using sensitive surface analysis and macrophage response was probed using RT-qPCR. This approach not only considers material degradation but also how macrophages respond to subsequent material properties. We used mechanochemical distress to more closely mimic physiological conditions rather than solely rely on static culture conditions as is the norm. This approach enabled us to observe different macrophage responses to mesh than those detected using static conditions alone. Our data shows mechanochemical distress causes physical changes to the surface of the PP surgical mesh that macrophages respond to with altered gene expression compared to control mesh. Macrophages in turn cause chemical oxidation of the mesh. This feed-forward relationship between the mesh surface condition and macrophages can only be demonstrated using provocation testing (deliberate mechano-oxidation) of the mesh. From the perspective of bringing advanced healthcare materials to the clinic, our work highlights the importance of incorporating improved *in vitro* testing methods.

## Funding

This work was supported by Engineering and Physical Sciences Research Council (EPSRC) [N.T.H.F grant: EP/T517835/1, N.T.H.F and C.R grant: EP/V012126/1]; Medical Research Council (MRC) through the Confidence in Concept scheme [N.T.H.F, S.S, C.R, S.R, C.C, V.H and S.M]; The Urology Foundation [S.S.].

## CRediT authorship contribution statement

**Nicholas T.H. Farr:** Writing – review & editing, Writing – original draft, Visualization, Validation, Supervision, Software, Resources, Project administration, Methodology, Investigation, Funding acquisition, Formal analysis, Data curation, Conceptualization. **Victoria L. Workman:** Writing – review & editing, Writing – original draft, Visualization, Validation, Supervision, Project administration, Methodology, Investigation, Formal analysis. **Sanad Saad:** Writing – review & editing, Writing – original draft, Visualization, Methodology, Investigation, Formal analysis, Data curation, Conceptualization. **Sabiniano Roman:** Writing – review & editing, Supervision, Data curation, Conceptualization. **Vanessa Hearnden:** Writing – review & editing, Supervision, Resources, Methodology, Funding acquisition, Conceptualization. **Christopher R. Chapple:** Writing – review & editing, Visualization, Supervision, Resources, Methodology, Funding acquisition, Conceptualization. **Craig Murdoch:** Writing – review & editing, Supervision, Resources, Methodology. **Cornelia Rodenburg:** Writing – review & editing, Supervision, Resources, Methodology, Funding acquisition, Conceptualization. **Sheila MacNeil:** Writing – review & editing, Visualization, Validation, Supervision, Resources, Methodology, Investigation, Funding acquisition, Conceptualization.

## Declaration of competing interest

The authors declare that they have no known competing financial interests or personal relationships that could have appeared to influence the work reported in this paper.

## Data availability

Data will be made available on request.

## Acknowledgments

N.T.H.F and C.R acknowledge the Sorby Centre for Electron Microscopy at the University of Sheffield for allowing electron microscopy and analysis to be performed. S.S, C.C, V.H and S.M would like the acknowledge the Luff Foundation for the fellowship awarded to S.S.

## Appendix A. Supplementary data

Supplementary data to this article can be found online at https://doi.org/10.1016/j.bioadv.2024.213800.

## References

[1] C. Crowley, et al., A systematic review on preclinical and clinical studies on the use of scaffolds for bone repair in skeletal defects, Curr. Stem Cell Res. Ther. 8 (3) (2013) 243–252.
[2] M. Geetha, et al., Ti based biomaterials, the ultimate choice for orthopaedic implants – a review, Prog. Mater. Sci. 54 (3) (2009) 397–425.
[3] D. Salthouse, et al., Interplay between biomaterials and the immune system: challenges and opportunities in regenerative medicine, Acta Biomater. 155 (2023) 1–18.
[4] S. Roman, et al., Use of a simple in vitro fatigue test to assess materials used in the surgical treatment of stress urinary incontinence and pelvic organ prolapse, Neurourol.Urodyn. 38 (1) (2019) 107–115.
[5] N.T.H. Farr, et al., A novel characterisation approach to reveal the mechano–chemical effects of oxidation and dynamic distension on polypropylene surgical mesh, RSC Adv. 11 (55) (2021) 34710–34723.
[6] C.R. Chapple, et al., Consensus statement of the European urology association and the European Urogynaecological association on the use of implanted materials for treating pelvic organ prolapse and stress urinary incontinence, Eur. Urol. 72 (3) (2017) 424–431.
[7] S. MacNeil, et al., Repairing the female pelvic floor: when good enough is not good enough, Nat. Rev. Urol. 15 (4) (2018) 197–198.
[8] N. Mangir, et al., Landmarks in vaginal mesh development: polypropylene mesh for treatment of SUI and POP, Nat. Rev. Urol. 16 (11) (2019) 675–689.
[9] D. Taylor, The failure of polypropylene surgical mesh in vivo, J. Mech. Behav. Biomed. Mater. 88 (2018) 370–376.
[10] N.T.H. Farr, Revealing localised Mechanochemistry of biomaterials using in situ multiscale chemical analysis, Materials 15 (10) (2022) 3462.
[11] A. Carnicer-Lombarte, et al., Foreign body reaction to implanted biomaterials and its impact in nerve Neuroprosthetics, Front. Bioeng. Biotechnol. 9 (2021) 622524.
[12] C. Zhang, M. Yang, A.C. Ericsson, Function of macrophages in disease: current understanding on molecular mechanisms, Front. Immunol. 12 (2021) 620510.
[13] J.M. Anderson, A. Rodriguez, D.T. Chang, Foreign body reaction to biomaterials, Semin. Immunol. 20 (2) (2008) 86–100.
[14] M.J. Wiggins, et al., Biodegradation of polyether polyurethane inner insulation in bipolar pacemaker leads, J. Biomed. Mater. Res. 58 (3) (2001) 302–307.
[15] R.S. Labow, E. Meek, J.P. Santerre, Hydrolytic degradation of poly(carbonate)-urethanes by monocyte-derived macrophages, Biomaterials 22 (22) (2001) 3025–3033.
[16] A. Dievernich, et al., Characterization of innate and adaptive immune cells involved in the foreign body reaction to polypropylene meshes in the human abdomen, Hernia 26 (1) (2022) 309–323.
[17] U. Klinge, A. Dievernich, J. Stegmaier, Quantitative characterization of macrophage, lymphocyte, and neutrophil subtypes within the foreign body granuloma of human mesh explants by 5-marker multiplex fluorescence microscopy, Front Med (Lausanne) 9 (2022) 777439.
[18] L. Li, et al., Pathological findings in explanted vaginal mesh, Hum. Pathol. 69 (2017) 46–54.
[19] A.L. Nolfi, et al., Host response to synthetic mesh in women with mesh complications, Am. J. Obstet. Gynecol. 215 (2) (2016), p. 206.e1-8.
[20] C.E. Witherel, et al., Macrophage and fibroblast interactions in biomaterial-mediated fibrosis, Adv. Healthc. Mater. 8 (4) (2019) e1801451.
[21] M. Jannasch, et al., A comparative multi-parametric in vitro model identifies the power of test conditions to predict the fibrotic tendency of a biomaterial, Sci. Rep. 7 (1) (2017) 1689.
[22] N. Grotenhuis, et al., In vitro model to study the biomaterial-dependent reaction of macrophages in an inflammatory environment, Br. J. Surg. 101 (8) (2014) 983–992.
[23] G. Zhou, et al., In vitro study of the host responses to model biomaterials via a fibroblast/macrophage co-culture system, Biomater. Sci. 5 (1) (2017) 141–152.
[24] T.M. Smith, et al., Pathologic evaluation of explanted vaginal mesh: interdisciplinary experience from a referral center, Female Pelvic Med. Reconstr. Surg. 19 (4) (2013) 238–241.
[25] K. Kocsy, et al., BS22 double positive (CD86+ MRC1+) inflammatory macrophages in the pathogenesis of carotid atherosclerosis, Heart 105 (Suppl. 6) (2019) A155.
[26] A. Dievernich, et al., Tissue remodeling macrophages morphologically dominate at the interface of polypropylene surgical meshes in the human abdomen, Hernia 24 (6) (2020) 1175–1189.
[27] S.E. Blatt, et al., Characterizing the macrophage response to immunomodulatory biomaterials through gene set analyses, Tissue Eng. Part C Methods 26 (3) (2020) 156–169.
[28] T.B. Wissing, et al., Macrophage-driven biomaterial degradation depends on scaffold microarchitecture, Front. Bioeng. Biotechnol. 7 (2019) 87.
[29] B. Klosterhalfen, K. Junge, U. Klinge, The lightweight and large porous mesh concept for hernia repair, Expert Rev. Med. Devices 2 (1) (2005) 103–117.
[30] B. Ollington, H.E. Colley, C. Murdoch, Immunoresponsive tissue-engineered Oral mucosal equivalents containing macrophages, Tissue Eng. Part C Methods 27 (8) (2021) 462–471.
[31] G. Fakhrullina, et al., Nanoscale imaging and characterization of Caenorhabditis elegans epicuticle using atomic force microscopy, Nanomedicine 13 (2) (2017) 483–491.
[32] N.T.H. Farr, et al., Characterization and quantification of oxidative stress induced particle debris from polypropylene surgical mesh, Nano Select 4 (6) (2023) 395–407.
[33] N.T.H. Farr, B. Klosterhalfen, G.K. Noé, Characterization in respect to degradation of titanium-coated polypropylene surgical mesh explanted from humans, J. Biomed. Mater. Res. B Appl. Biomater. 111 (5) (2023) 1142–1152.
[34] A.J. Wood, et al., Materials characterization and histological analysis of explanted polypropylene, PTFE, and PET hernia meshes from an individual patient, J. Mater. Sci. Mater. Med. 24 (4) (2013) 1113–1122.
[35] A. Imel, et al., In vivo oxidative degradation of polypropylene pelvic mesh, Biomaterials 73 (2015) 131–141.
[36] T. Jain, et al., Accelerated in vitro oxidative degradation testing of polypropylene surgical mesh, J. Biomed. Mater. Res. B Appl. Biomater. 111 (12) (2023) 2064–2076.
[37] H. Tadokoro, et al., Normal vibrations of the Polymer molecules of helical conformation. V. Isotactic polypropylene and its Deuteroderivatives, J. Chem. Phys. 42 (1965) 1432–1449.
[38] A.S. Nielsen, D.N. Batchelder, R. Pyrz, Estimation of crystallinity of isotactic polypropylene using Raman spectroscopy, Polymer 43 (9) (2002) 2671–2676.
[39] B. Gewert, M.M. Plassmann, M. MacLeod, Pathways for degradation of plastic polymers floating in the marine environment, Environ. Sci.: Processes Impacts 17 (9) (2015) 1513–1521.
[40] C. Vasile, Handbook of Polyolefins, CRC Press, 2000.
[41] M. Geiser, S. Schurch, P. Gehr, Influence of surface chemistry and topography of particles on their immersion into the lung's surface-lining layer, J. Appl. Physiol. 94 (5) (1985) 1793–1801.
[42] S.L. Wright, F.J. Kelly, Plastic and human health: a Micro issue? Environ. Sci. Technol. 51 (12) (2017) 6634–6647.
[43] J. Hwang, et al., An assessment of the toxicity of polypropylene microplastics in human derived cells, Sci. Total Environ. 684 (2019) 657–669.

[44] H. Kress, et al., Filopodia act as phagocytic tentacles and pull with discrete steps and a load-dependent velocity, Proc. Natl. Acad. Sci. U. S. A. 104 (28) (2007) 11633–11638.
[45] H. Schachtner, et al., Podosomes in adhesion, migration, mechanosensing and matrix remodeling, Cytoskeleton 70 (10) (2013) 572–589.
[46] W.J. Kao, et al., Theoretical analysis of in vivo macrophage adhesion and foreign body gaint cell formation on polydimethylsiloxane, low density polyethylene, and polyetherurethanes, J. Biomed. Mater. Res. 28 (1) (1994) 73–79.
[47] Q.H. Zhao, et al., Human plasma alpha 2-macroglobulin promotes in vitro oxidative stress cracking of Pellethane 2363-80A: in vivo and in vitro correlations, J. Biomed. Mater. Res. 27 (3) (1993) 379–388.
[48] M. Schnoor, et al., Production of type VI collagen by human macrophages: a new dimension in macrophage functional Heterogeneity1 2, J. Immunol. 180 (8) (2008) 5707–5719.
[49] T. Furukawa, et al., Molecular structure, crystallinity and morphology of polyethylene/ polypropylene blends studied by Raman mapping, scanning Electron microscopy, wide angle X-ray diffraction, and differential scanning calorimetry, Polym. J. 38 (11) (2006) 1127–1136.
[50] A.J. Satti, et al., Morphological Raman analysis of short chain branched ethylene and propylene metallocenic copolymers, Polym. Test. 67 (2018) 450–456.
[51] G. Masetti, F. Cabassi, G. Zerbi, Vibrational spectrum of syndiotactic polypropylene. Raman tacticity bands and local structures of iso- and syndiotactic polypropylenes, Polymer 21 (2) (1980) 143–152.
[52] A. Shyichuk, D. Stavychna, J. White, Effect of tensile stress on chain scission and crosslinking during photo-oxidation of polypropylene, Polym. Degrad. Stab. 72 (2) (2001) 279–285.
[53] M. Chanda, S.K. Roy, Plastics Technology Handbook, 4th ed, CRC Press, 2006.
[54] B. Fayolle, L. Audouin, J. Verdu, Oxidation induced embrittlement in polypropylene — a tensile testing study, Polym. Degrad. Stab. 70 (3) (2000) 333–340.
[55] H.J. Oswald, E. Turi, The deterioration of polypropylene by oxidative degradation, Polym. Eng. Sci. 5 (3) (1965) 152–158.
[56] V.V. Iakovlev, S.A. Guelcher, R. Bendavid, Degradation of polypropylene in vivo: a microscopic analysis of meshes explanted from patients, J. Biomed. Mater. Res. B Appl. Biomater. 105 (2) (2017) 237–248.
[57] J.C.W. Chien, C.R. Boss, Polymer reactions. V., Kinetics of autoxidation of polypropylene, Journal of Polymer Science Part A-1 5 (12) (1967) 3091–3101.
[58] A.D. Talley, et al., Oxidation and degradation of polypropylene transvaginal mesh, J. Biomater. Sci. Polym. Ed. 28 (5) (2017) 444–458.
[59] A.C. Trombetta, et al., A circulating cell population showing both M1 and M2 monocyte/macrophage surface markers characterizes systemic sclerosis patients with lung involvement, Respir. Res. 19 (1) (2018) 186.
[60] K.S. Jones, Effects of biomaterial-induced inflammation on fibrosis and rejection, Semin. Immunol. 20 (2) (2008) 130–136.
[61] X.M. Meng, D.J. Nikolic-Paterson, H.Y. Lan, TGF-β: the master regulator of fibrosis, Nat. Rev. Nephrol. 12 (6) (2016) 325–338.
[62] S. O'Reilly, et al., Interleukin-6 (IL-6) trans signaling drives a STAT3-dependent pathway that leads to hyperactive transforming growth factor-β (TGF-β) signaling promoting SMAD3 activation and fibrosis via gremlin protein, J. Biol. Chem. 289 (14) (2014) 9952–9960.
[63] X. Shi, et al., Transforming growth factor-β signaling in fibrotic diseases and Cancer-associated fibroblasts, Biomolecules 10 (12) (2020).
[64] W. Liu, et al., Interleukin 1beta (IL1B) signaling is a critical component of radiation-induced skin fibrosis, Radiat. Res. 165 (2) (2006) 181–191.
[65] Y. Li, et al., The role of IL-6 in fibrotic diseases: molecular and cellular mechanisms, Int. J. Biol. Sci. 18 (14) (2022) 5405–5414.
[66] L.A. Borthwick, The IL-1 cytokine family and its role in inflammation and fibrosis in the lung, Semin. Immunopathol. 38 (4) (2016) 517–534.
[67] L.K. Lundblad, et al., Tumor necrosis factor-alpha overexpression in lung disease: a single cause behind a complex phenotype, Am. J. Respir. Crit. Care Med. 171 (12) (2005) 1363–1370.
[68] C.G. Lee, et al., Transgenic overexpression of interleukin (IL)-10 in the lung causes mucus metaplasia, tissue inflammation, and airway remodeling via IL-13-dependent and -independent pathways, J. Biol. Chem. 277 (38) (2002) 35466–35474.
[69] B.N. Brown, et al., Characterization of the host inflammatory response following implantation of prolapse mesh in rhesus macaque, Am. J. Obstet. Gynecol. 213 (5) (2015), p. 668.e1-10.
[70] A. Yabluchanskiy, et al., Matrix metalloproteinase-9: many shades of function in cardiovascular disease, Physiology (Bethesda) 28 (6) (2013) 391–403.
[71] C.Y. Cheng, et al., IL-1beta induces expression of matrix metalloproteinase-9 and cell migration via a c-Src-dependent, growth factor receptor transactivation in A549 cells, Br. J. Pharmacol. 160 (7) (2010) 1595–1610.
[72] H.N. Wilkinson, M.J. Hardman, Wound healing: cellular mechanisms and pathological outcomes, Open Biol. 10 (9) (2020) 200223.